energies

MDPI

Article

Optimising Flowback Strategies in Unconventional Reservoirs: The Critical Role of Capillary Forces and Fluid Dynamics

Hamid Reza Nasriani [1], Mahmoud Jamiolahmady[2]

[1] School of Engineering & Computing, University of Central Lancashire, Preston, PR1 2HE, United Kingdom; hrnasriani@uclan.ac.uk
[2] Heriot-Watt University, Institute of Geoenergy Engineering, Edinburgh, United Kingdom
* Correspondence: hrnasriani@uclan.ac.uk

Abstract: This study delves into the complexities of fluid cleanup processes post-hydraulic fracturing in unconventional gas deposits, focusing on the pivotal role of capillary pressure (Pc) correlations in tight and ultra-tight formations. Utilising the Geo2Flow software, the research evaluates the efficacy of existing Pc models, identifying the Brooks & Corey model as notably precise for these formations, albeit recommending an adjustment to the pore size distribution index for a more accurate representation of rock behaviours. Further investigation centres on the cleanup process in multiple fractured horizontal wells, examining the impact of Pc, matrix permeability, drawdown pressure, and fracturing fluid volume. A significant portion of the study addresses the influence of interfacial tension-reducing chemicals on post-fracturing production, highlighting their utility in ultra-tight formations but advising against their use in tight formations due to environmental concerns and limited efficacy. The findings underscore the nuanced interplay between geological parameters and fracturing fluid dynamics, advocating for tailored fluid cleanup strategies that enhance hydraulic fracturing efficiency while minimising environmental impact. This comprehensive analysis offers valuable insights into optimising fracture cleanup and understanding the underlying physics, thereby contributing to more effective hydraulic fracturing practices.

Keywords: Flowback cleanup; Hydraulic Fracturing; fracturing fluid; Capillary pressure; IFT; unconventional reservoirs.

Citation: To be added by editorial staff during production.

Academic Editor: Firstname Lastname

Received: date
Revised: date
Accepted: date
Published: date

1. Introduction

The least polluting and emitting fossil fuel is thought to be natural gas. Due to its abundance and environmental sustainability, it is also regarded as one of the most significant energy sources in the future. Around the world, using natural gas is becoming increasingly significant in producing electricity, industrial processes, and domestic heating. Resources for natural gas are either conventional or unconventional. Despite being less economically viable than conventional natural gas reserves and more challenging to extract, there is a rising reliance on unconventional gas resources to meet the world's energy demands. Shale gas, gas hydrates, tight and ultra-tight gas sands and coalbed methane are all sources of unconventional gas plays. The considerable rise in gas consumption has led to the development of further unconventional resources[1–3].

Fracturing, or hydraulic fracturing, is a prevailing technique for increasing the production of wells in unconventional gas reserves. With this technique, the rock formation is fractured by pumping a mixture of water, chemicals and sand into the well under significant pressure. Different companies have widely adopted Fracturingor, which extracts large quantities of natural gas from unconventional deposits, but it has also been met with opposition due to environmental and health concerns[4–13].

Shale gas and tight gas sands are gaining popularity among unconventional resources. Conversely, conventional natural gas reserves are exhausted because of their availability and relative ease of access [14–20].

The potential benefits and disadvantages of natural gas unconventional resources need to be weighed against the larger picture of global energy demands and environmental concerns. The environmental impact of extracting unconventional gas resources and the possible health implications must be handled and examined, notwithstanding the resource's promise as a supply of natural gas. Companies and governments are developing new technologies and laws to meet energy demands while lowering their negative effects on the environment. Unconventional resources, thus, play a progressively essential role in addressing global energy demands, notwithstanding the difficulties they provide compared to conventional reserves. Technologies and techniques, such as hydraulic fracturing, are being developed to enhance the production of unconventional gas resources while minimising environmental impact. As the world continues to face energy challenges, it is crucial to consider the potential benefits and drawbacks of unconventional natural gas resources in the context of the bigger picture of global energy demands and environmental concerns [14–20].

Injecting large amounts of fracturing fluid, or FF, allows for initiation and propagating cracks in unconventional reservoirs[21–26]. In the tight oil and gas sectors, vertically drilled, hydraulically fractured wells have first been drilled in Pennsylvania, a state in the northeastern United States. Numerous experimental, computational, and field studies have been conducted to determine how hydraulic fracture cleanup effectiveness affects phase production in unconventional tight/ultra-tight formations [21,22]. Numerous field experiments have demonstrated how considerably gas output can be hampered by inadequate FF removal.[27,28].

The physical characteristics of the FF, the formation's characteristics, and the hydraulic fracturing operation's design all affect the volume of the flowback. 10 to 70 percent of the entire volume of the initially injected FF could make up for the flowback recovered from the well at the surface[29,30]. More FF is often retained in the formation. Therefore, when the formation has some micro fractures and higher matrix capillary pressures, surface flowback recovery is reduced [29,30].

The oil and gas sector now emphasises optimising the fracturing fluid flowback for a number of purposes such as maximising net profit and addressing environmental concerns. Some techniques mitigate FF flowback using a Tech-Flo hydraulic jet pump to maximise load recovery [31]. Simultaneously isolating the hydrocarbon from the well stream helps hasten the safe recovery of a substantial flowback. A flowback service for multiple fractured horizontal wells (MFHWs) in unconventional fields has also been made available by Halliburton[32]. CALIBR, a service offered by a company called CALIBR, aims to boost well performance by reducing completion damage and maximising long-term output. The service enhances productivity and completion efficiency by continuously monitoring, analysing, and controlling flowback. Through the use of CALIBR, hazardous flowback procedures can be avoided, the damage in fracture permeability can be reduced, and the performance of the well can be improved. This is achieved by continuously monitoring well pressure, assessing well performance, and adjusting the choke in real-time. CALIBR, a flowback operation service by Halliburton, enhances well performance by reducing completion damage and maximising long-term output. This service employs real-time monitoring and analysis using high-resolution pressure gauges like SPIDR®, allowing for precise adjustments to flowback processes based on continuous data acquisition. Each flowback plan is customised to the well's specific characteristics, incorporating its design, previous completion activities, and field knowledge to optimise productivity and minimise damage. Through an iterative process of continuous measurement, analysis, and choke adjustment, CALIBR avoids aggressive flowback strategies that could damage fracture conductivity, thus maintaining well performance. Additionally, the service mitigates potential damage-causing practices, reducing the risk of issues such as proppant washout and fines migration. Overall, CALIBR's comprehensive, data-driven approach to flowback management maximises the economic value and long-term productivity of wells[32] . Holditch [25] studied how the productivity of fractured wells is affected by the growth of fluid saturation (FF), which is assumed to be water, and the reduction of permeability in the area near the fracture. His goal was to determine the impact of damage to the grid-like structure surrounding the fracture. He used a numerical simulator based on finite differences to conduct his research. It was found that in low-pressure drawdown conditions, where the drawdown pressure (DP) was only slightly greater than the capillary pressure (Pc) of the matrix in tight formations (reservoirs with low permeability), the effect of capillary pressure was significant. He pointed out that water blocking takes place when the matrix permeability(km) around the fracture declines by 99.9%, or when the differential pressure (DP) is less than the capillary pressure (Pc) in the region where the fracturing fluid (FF) has penetrated. The invasion depth of the FF in their matrix extended up to 5 inches, and its distribution within the matrix adjacent to the hydraulic fracture was consistent. His study did not examine the impact of FF volume on the conductivity of the fracture.

Decline in expected gas production is a complex process involving several factors, including matrix permeability damage caused by two-phase flow and the efficacy of cleaning up single fractured vertical wells. To understand these factors, researchers have conducted extensive studies that have shed light on the underlying mechanisms that affect gas productivity.

One important finding is that Pc and Kr in invaded zones are important factors in cleanup effectiveness in low-permeability reservoir rocks. This conclusion was drawn by Pope et al. in 1996, who determined a direct correlation between gas flow and flowback recovery by analysing data taken from the field. They suggested that when the liquid is produced from the hydraulic fracture, a corresponding space opens up, allowing gas to flow towards the well. As load recovery increases, gas production also upsurges. To further investigate this, they examined the dependency of gas rates on flowback and advised that higher flow rates leads to higher load fluid recovery.

Following their investigation, Gdanski et al. [28] examined the formation damage caused by gas and fluid flow in the invaded zone and established a numerical model. They noticed that damages in the fracture sand face significantly lower gas productivity if the permeability of the matrix in the invaded zone is reduced to 1% of the original permeability. However, they overlooked that higher Pc results in more fluid being absorbed into the matrix, which lowers fluid saturation within the frack, increases the permeability of gas within the fracture, and produces cleaner fractures.

The next important factor in gas production is the effectiveness of cleaning up fractured wells. Ghahri et al. investigated this issue in 2009 and understood that cleaning up such wells in gas fields efficiently enhances gas productivity. Their findings were based on a numerical simulations and detailed analysis of field data and they proven that cleaning up single fractured vertical wells can lead to significant improvements in gas recovery.

These findings highlight the complex nature of gas production and the need to understand the underlying mechanisms that affect productivity. By building on the work of earlier researchers, current and future studies can continue to shed light on this important issue, aiming to improve gas recovery and meet the world's growing energy needs.

Additionally, they replicated the numerically developed model outcomes that Holditch (1979) indicated, which have since been used as a reference in several cleanup simulation investigations[25]. According to their findings, the presence of FF in the zone that has been invaded influences the total amount of gas recovery by diminishing the relative permeability of the gas, which reduces gas rate when in contrast to a scenario in which FF was not pumped into the well. More significant FF recovery occurs during production when FF viscosity is reduced and, as a result, FF mobility is increased. They also emphasised that as Pc rises, the FF penetrates deeper into the matrix, improving gas production and reducing FF interference.

Ghahri et al (2011) expanded on this study by thoroughly examining 16 important parameters while utilising experimental design and a surface model [33]. They showed that the parameters relating to the FF cleanup within the fracture, particularly kf, had a considerable impact on gas production loss, or GPL[33].

The central processing unit (CPU) time needed for these two numerical experiments was excessive [33]. As a result, the authors could only examine two simulation sets. Jamiolahmady et al. (2014) conducted additional research on flowback cleanup processes. They simplified the model by reducing the number of parameters from 16 to 12 by removing four parameters that had minimal impact on the cleanup performance. This made it easier to explore more diverse cleanup scenarios.

The study that was conducted by Ghahri et al (2011) focused on different factors that included the size of the pores, the force between interfaces, how easy it is for substances to pass through the matrix and fracture, and the way that fluids move through these structures. The study was expanded to cover a wider variety of cleanup situations in gas reservoirs that are extremely tight. To achieve this, researchers ran eighty-four simulations that considered various factors, such as the amount of fluid injected, the duration of the soak, the pressure at the bottom of the well, and the compactness of the formation [33].

The study revealed that the cleanup process becomes slower and gas production loss becomes more significant as the formation becomes tighter (i.e., smaller km). Likewise, the study demonstrated that when the pressure drawdown was low, the capillary pressure (Pc) more significantly impacted the efficiency of the cleanup process than before. A similar result was obtained when the soaking period was increased. Nasriani and colleagues have conducted several studies on enhanced oil recovery, investigating various techniques and strategies ([29,30,34–39]), while more recent works by Modebelu et al. (2022) & Erimako et al. (2022) have focused on particular aspects of the process[40,41]. Nasriani et al. (2018) studied various factors impacting post-fracturing cleanup effectiveness [30,36]. The study considered several variables, such as the length of the fracture, well pressure, hysteresis, segregation due to gravity, mobility, immobility of the connate water, and volume of the injected fracture fluid. The results of the investigation revealed that particular outcomes may arise when a considerable quantity of fracture fluid is injected into formations with extremely high permeability, it significantly reduces gas flow and severely slows the cleanup procedure. Extending the soaking time or increasing the pressure drawdown did little improve GPL in this situation. The researchers found that hysteresis did not significantly affect the efficiency of the cleanup process. The examination of cleanup performance was extended to explore the influence of layered systems, and it was discovered that capillary pressure plays a more crucial role in the bottom layer than in the top layers. Additionally, The mobility coefficient of the fluid in the fracture is higher in the upper layer than in the lower layer. Furthermore, they suggested that using an IFT reduction agent during fracturing operations could reduce gas production losses in reservoirs with high water saturation levels.

Nasriani and Jamiolahmady (2019) expanded the research scope to include studies to conduct to examine the cleanup procedure that takes place after hydraulic fracturing in wells with multiple horizontal fractures [29].

More precisely, the effect of wide-ranging horizontal lengths and fracture spacing in MFHWs on cleanup efficiency was studied. Furthermore, the researchers compared the cleanup processes after fracturing in vertical wells (VWs) and MFHWs. Running the numerical simulation for the sets consumed considerable CPU time.

In an effort to mitigate the significant computational burden associated with simulation runs using full factorial sampling (FFS) experimental design and to accelerate the computational process, researchers have adopted an alternative approach known as Latin Hypercube Sampling (LHS). This novel sampling technique has emerged as a promising solution for conducting high-dimensional experiments with fewer runs, thereby reducing the overall CPU time required for simulation. They observed a difference in the trend of km values between the base reference set and the VW Set for multiple fractured horizontal wells. The researchers identified that the shift in flow geometry and well completion technique resulted in a shift in the trend of km in the set to a positive coefficient value, previously it was observed that Km coefficient was negative in vertical wells. Additionally, they discovered that capillary pressure (Pc) variables played a more crucial role in the sets, while the Corey pertinent parameters for relative permeability models for both gas and FF in both matrix and fracture were further impactful in the vertical wells.

According to these results, FF production was more adversely impacted gas production in the set. In simpler terms, a greater Pc in MFHWs is more significant since it causes more FF to get more absorbed into the rock and less opposition to gas passage. It was also demonstrated that MFHW cleaned up more quickly than VW. This resulted from sets having a greater gas production rate. Slower (faster) cleanup was seen in Reduced (Increased) DP MFHW settings, comparable to those formerly reported for the related VW sets. They concluded that while fracture interference and fracture spacing substantially impact flow, they have little effect on cleanup performance in MFHWs with varying spacing between fractures.

Recent advancements in hydraulic fracturing and unconventional gas extraction have significantly contributed to the efficiency and productivity of shale gas reservoirs. For instance, characterising anisotropic geomechanical properties through nanoindentation and upscaling approaches provides a deeper understanding of formation behaviour, which is critical for optimising hydraulic fracturing treatments [42]. Additionally, computational analyses of proppant transport and screen-out phenomena have highlighted the complex interactions within fractures, leading to more effective fracturing strategies [43]. Experimental studies on the stable dispersion of coal fines during hydraulic fracturing flowback emphasise the importance of addressing particle mobilisation to enhance cleanup efficiency [44]. Furthermore, probabilistic quantification of microparticle segregation under electrostatic forces has provided new insights into preventing screen-out during fracturing operations [45]. Innovative techniques such as co-applicating indirect hydraulic fracturing and micro-proppants have improved pre-drainage in low permeability coals, highlighting the ongoing efforts to enhance gas recovery in challenging formations [46].

Moreover, the integration of machine learning in reservoir management has opened new avenues for predicting production and optimising resource extraction. Srinivasan et al. (2021) demonstrated the potential of machine learning-assisted history matching and production forecasting in shale gas reservoirs, which can significantly improve decision-making processes and operational efficiency [47]. These recent studies collectively underscore the critical role of technological advancements and interdisciplinary research in addressing the challenges of unconventional gas production, thereby supporting the growing global energy demands while mitigating environmental impacts.

This study aims to enhance the existing knowledge of hydraulic fracturing treatments for real-world applications by building on prior research [3,14,15,20,30,31]. It specifically explores the influence of unconventional Pc on the performance of MFHWs. This paper presents an in-depth analysis of Pc correlations applicable to tight and ultra-tight formations, utilising the Geo2Flow software. Geo2Flow is an advanced numerical modeling framework that integrates petrophysical, geological, engineering, and geophysical data to accurately simulate groundwater flow and solute transport in porous media. By matching 3D saturations to well logs, calculating precise 3D permeabilities, and identifying reservoir compartments, Geo2Flow enhances the accuracy of reserve estimations and subsurface models. Its interdisciplinary approach and robust algorithms ensure that it handles both data-rich and data-poor environments effectively, making it a valuable tool for environmental engineers and researchers[48].

Analysis of the Pc model, applied to 200 datasets from conventional, tight, and ultra-tight formations, proved that the Brooks & Corey model, with just one specific parameter, effectively represents Pc data for unconventional plays. Results from this research recommend constraining the pore size distribution index (λ) to a 0.3–1.5 range for a more accurate portrayal of unconventional rock properties. The updated λ range was incorporated into the model to more accurately represent the unconventional Pc characteristics.

Additionally, for these five data sets, a novel dimensionless terminology—analogous to gas production loss (GPL)—was introduced to study the influence of similar key parameters on FF production, which is a significant factor in the HF of unconventional reservoirs.

2. Methodology

A flowchart is used in this part to clarify the adopted analysis methodologies and terminologies, as shown in Figure 1. A comprehensive assessment of capillary pressure (Pc) correlations for tight and ultra-tight formations has been conducted.This analysis utilised the Geo2Flow software to examine the dependability of existing Pc correlation models specifically for these formations [41,48]. Then, it was decided that Pc data would be best represented by Brooks and Corey's model. in unconventional plays. However, it was proved for the first time that the λ range for unconventional resources used in the Brooks and Corey model must be adjusted to 0.3 to 1.5, rather than 1 to 4 previously used in previous works [30]. This Pc formulation adjustment improves capillary forces' representation in unconventional tight/ultra-tight rock formations more realistically. Then, a multiple horizontal fractured well model initially created by [29] was utilised for sets. The dimension of the model is shown in Table 1; the validation procedure of the modified MFHW model is discussed elsewhere. [30].

Once the MFHW model is validated, five scenarios are considered. The five different scenarios are:

Scenario 1. Base reference set
Scenario 2. A set with the modified Λ range
Scenario 3. A set with different injected FF
Scenario 4. A set with different Km range
Scenario 5. A set with larger drawdown

It should be highlighted that each set consists of 1000 simulation runs in which the 12 pertinent parameters are varied within their variation range. The range of all pertinent parameters is shown in Table 2. A full explanation of the sampling approaches used in this work can be found elsewhere [29]. All scenarios used Latin Hypercube Sampling (LHS) to generate the required simulation runs, and then mathematical surface methodology was used to match an accurate model to the results from each set. Finally, results from these sets were examined. A list of sets that have been analysed is shown in Table 3.

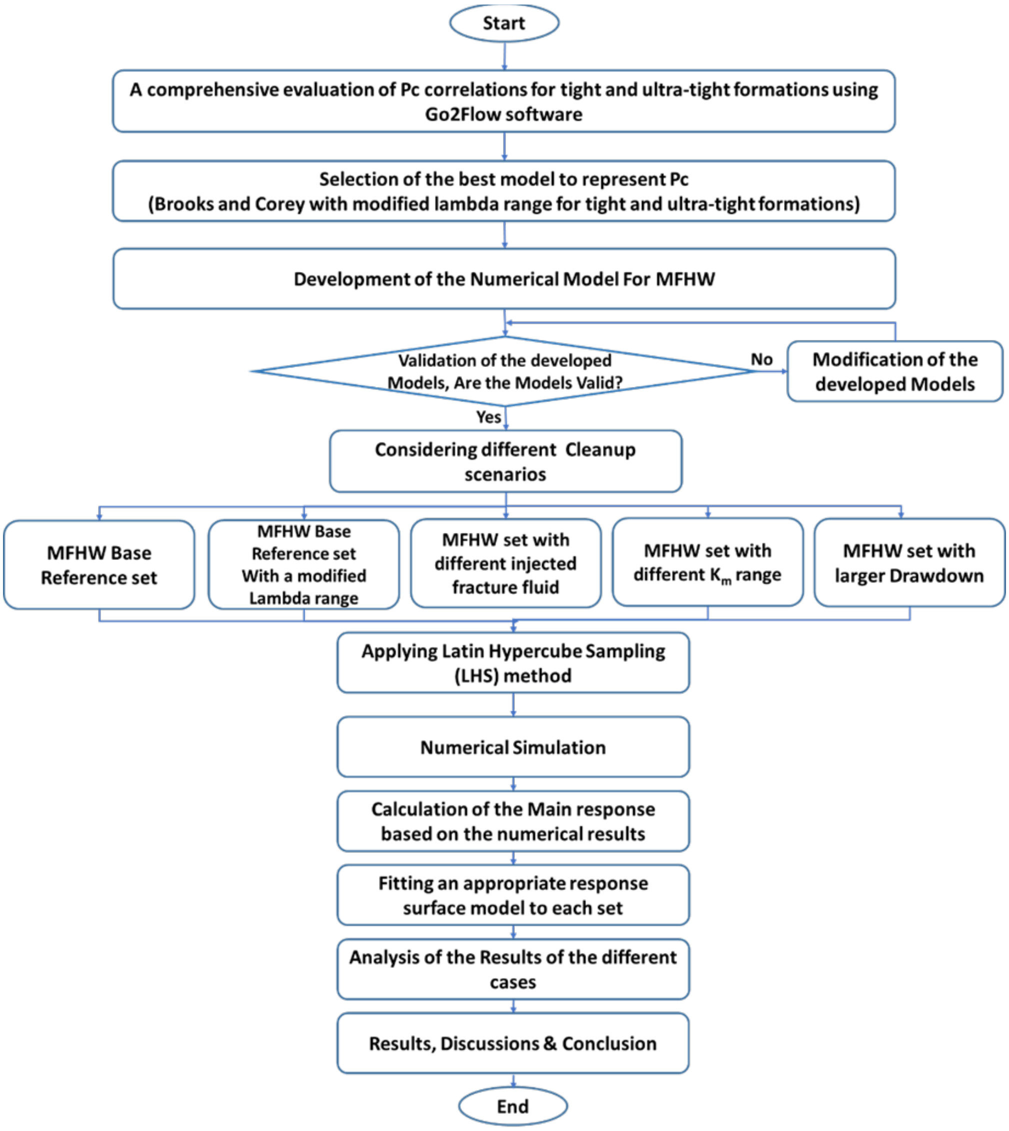

Figure 1 the workflow of the study

Table 1 MFHW model

Lf(m)	wf(m)	Horizontal length (m)	Number of Fractures	Xres(m)	Yres(m)	Zres(m)
90	0.004	600	7	2000	2000	40

Table 2 The parameters' variation range

Parameter	Min	Max
k_f (D)	1	30
k_m	1 μD	100 μD
λ	1	4
IFT (mNm/m)	2	50
n_{gm}	1.5	5
n_{wm}	1.2	4
k_{maxg}	0.5	1.0
k_{maxw}	0.05	0.6

n_{gf}	1.5	5
n_{wf}	1.2	4
k_{maxg}	0.5	1.0
k_{maxw}	0.1	0.75

Table 3 MFHW Set analysed.

Set Name	No. of fracks	Horizontal Length (m)	DP (Psi)	FVR	Shut-in time (days)	k_f (D)	k_m (µD)	lam	Sampling Approach	Number of Runs
Default Values	7	600	1000	2	2	1-30	1-100	1-4	LHS	1000
Set 8	✓	✓	✓	✓	✓	✓	✓	✓	✓	✓
Set 30	✓	✓	✓	✓	✓	✓	✓	0.3-1.5	✓	✓
Set 31	✓	✓	✓	✓	✓	✓	0.01-1	✓	✓	✓
Set 32	✓	✓	✓	10	✓	✓	✓	✓	✓	✓
Set 33	✓	✓	4000	✓	✓	✓	✓	✓	✓	✓

2.1 An in-depth assessment of Pc formulas in unconventional plays.

his section presents the findings from a comprehensive analysis of different Pc correlations applied to unconventional formations, utilising the Geo2Flow software. [39]. For this research, 200 Pc data sets, collected from tight and ultra-tight formations in western U.S. basins, were examined, with measurements provided by the University of Kansas Center for Research and presented to the U.S. Department of Energy [40].

The study specifically examined various J-function models to investigate capillary force irregularities in tight and ultra-tight sands. This part discusses the initial and adapted Leverett J-functions , other J-function models, and the associated fit error indicators as applied to these unconventional formations.

2.1.1.The Leverett J-function

Leverett (1941) showed that in reservoir rocks with identical lithology but varying porosity and permeability, capillary pressure could be normalised using a single function known as the Leverett J-Function. Rather than plotting Pc against Sw, Leverett instead used the J-Function, as detailed in Equation 1 [41].

$$J(S_w) = \frac{P_c}{\gamma cos\theta}\sqrt{\frac{k}{\varphi}} \qquad 1$$

Where γ is the Surface tension, θ is Contact angle, k is the Permeability and φ is the Porosity.

According to Leverett's method, a small set of J-functions can effectively represent the Pc characteristics across the rocks within an entire reservoir. Leverett's findings imply that, for a specific rock type, most Pc curves can align with one J-function. Essentially, one J-function can encompass multiple Pc curves.

2.1.2. J-function Displacement, Jd

the threshold value that the non-wetting phase must surpass to penetrate the rock is represented by the J-function displacement, Jd. This value aligns with the displacement pressure, P_d (also referred to as threshold pressure, P_e), as outlined in Equation 3.6 on the Pc curve. When P_d is substituted into Equation 5.1, J_d is obtained. In this study, all P_c functions are dependent on Jd, as it establishes the location of fluid contacts.

2.1.3. The Model proposed by Thomeer

In 1960, Thomeer demonstrated that plotting the logarithm of capillary pressure against the logarithm of saturation of non-wetting phase produces a hyperbolic curve.He introduced a J-function model, detailed in Equation 2 [42], to represent this relationship.

$$S = 1 - 10^{-\left(\frac{G}{Log\left(\frac{J}{J_d}\right)}\right)} \quad 2$$

Where S is reduced saturation, J_d is J-function displacement, J is the J-function value and G is the Pore geometric factor.

2.1.4. The J-function Model proposed by Brooks-Corey

Brooks and Corey (1966, 1964) developed a model using a bundle of capillary tubes to characterize a porous media, introducing the following terms [49,50]:

$$S = \left(\frac{J_d}{J}\right)^{\lambda} = \left(\frac{J_d}{J}\right)^{1/a_0} \quad 3$$

Equation 5.3 corresponds to Equations 3.6 and 3.7 on the capillary pressure curve.

2.1.5 The J-function Model proposed by Bentsen-Anli

Bentsen and Anli (1977) suggested a J-function model introduced by Eq.4 [51].

$$S = e^{\left(\frac{J_d - J}{a_0}\right)} \quad 1$$

2.1.6. The model of Skelt-Harrison

Skelt & Harrison (1995) proposed a J-function model characterized by two specific parameters, detailed in Equation 5 [46]. In contrast to the previous models, this model uniquely incorporates two parameters: a0, serving as the scaling factor for Pc, and a1, which functions as the exponent for the scaled Pc.

$$S = 1 - e^{-\left(\frac{a_0}{J - J_d}\right)^{a_1}} \quad 5$$

Skelt and Harrison first presented their model relating height above the free water level and Pc. Reformulating this relationship through the J-function yields Equation 5.

2.1.7. O'Meara Unimodal J approch

Similar to the the Skelt-Harrison J-function model, the O'Meara Unimodal J-function model incorporates two distinct parameters of a0 and a1, and is represented by Equation 6.

$$S = \frac{1}{2}\, erfc\left(\frac{Log\left(\frac{J - J_d}{a_0}\right)}{a_1}\right) \quad 6$$

In O'Meara's model, the erfc function denotes the complementary error function. This model is characterized by two distinct parameters: a0, which signifies the median of the associated lognormal distribution, and a1, which indicates the variance of that distribution.

2.2. Analysis of Pc Correlations

To evaluate the appropriateness of specified Pc correlations for ultra-tight rocks, 200 Pc datasets were integrated into Geo2Flow. In Geo2Flow software [39], data fit quality is determined through either the the least absolute deviations approach or least squares technique, with both assessed by an 'error in fit.' This error metric, applied to n data points (xi, yi) following the function y = f(x), is calculated as the sum of squared deviations between actual data points and their corresponding values when using the least squares method, as outlined in Equation 7

$$\Delta = \sum_{i=1}^{n} [y_i - f(x_i)]^2 \quad 7$$

In the case of the least absolute deviations (LAD)approach, the error is defined as the total of the absolute differences between the data points and their respective corresponding values, as indicated by Equation 8:

$$\Delta = \sum_{i=1}^{n} |y_i - f(x_i)| \quad 2$$

Notably, a lower Δ value indicates an improved curve fit. This work utilised the least squares method (LSM). For this task, all datasets were initially formatted in Excel to align with the requirements of Geo2Flow before importing into the software. Five different models were examined: Figure 2 illustrates the imported PC data sets in relation to saturation, with Pc expressed in Bar. The corresponding J-functions, derived using specific K, φ, IFT, and contact angle values, are displayed in Figure 3.

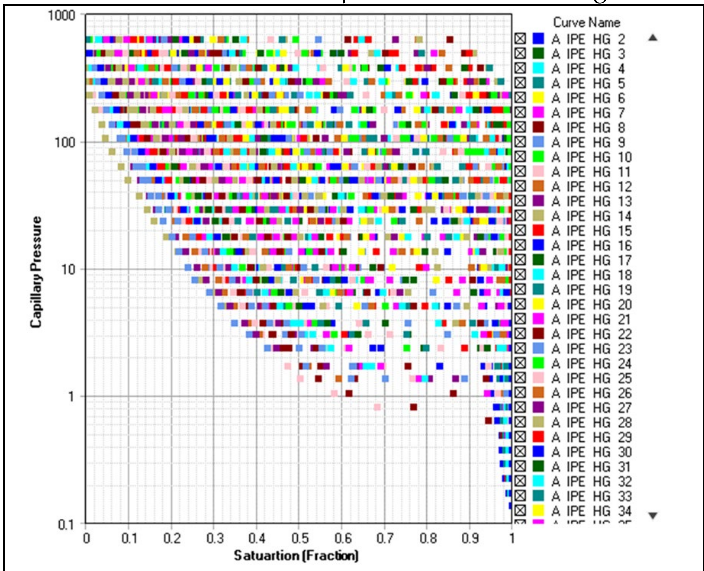

Figure 2 200 Pc vs saturation. (Pc in Bar)

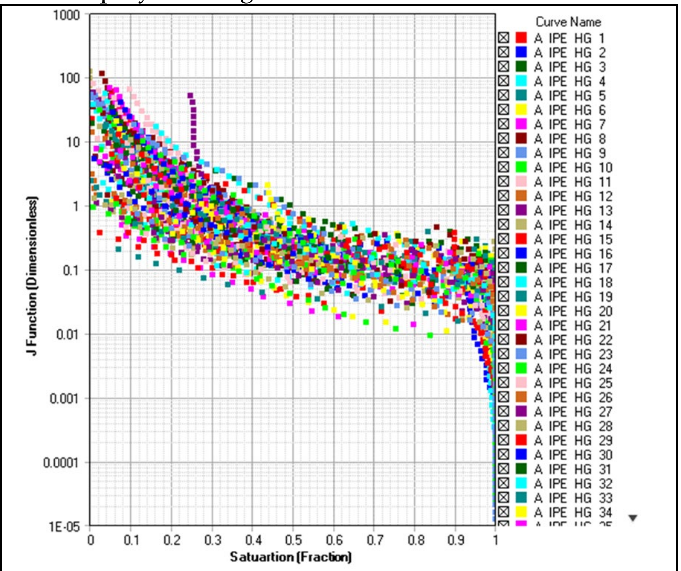

Figure 3 J-functions vs Sw

Five different models were evaluated: three single-parameter models (Brooks & Corey, Thomeer and Bentsen & Anli) and two dual-parameter models (Skelt-Harrison & O'Meara Unimodal). The Pc data sets were fitted using the least squares method (LSM), with the associated fit error values for each model outlined in Table 4. For the full data set, Table 4 presents the error values for the the five models. The Thomeer model, notably, provided the most accurate fit, while the Bentsen and Anli model had the highest error when assessing all data. Models with dual parameters generally produced more precise Pc predictions due to their greater adaptability; however, the Thomeer model, despite being a single-parameter model, performed better than many others. The Brooks and Corey model was the second most accurate among the single-parameter models.To improve the assessment of these models' reliability in unconventional formations, the Pc data sets were divided into three categories: conventional (k > 0.1 md), tight (0.001 < K < 0.1 md), and ultra-tight (K < 0.001 md), with the conventional data sets being excluded from further analysis. The LSM was reapplied to the unconventional data, and the resulting error values for each model are shown in Table 4. For tight Pc data, Table 4 includes the error values for the Thomeer, Brooks & Corey, Bentsen & Anli, Skelt-Harrison, and O'Meara models. The Brooks & Corey model was found to be the most accurate among single-parameter models, while the Skelt-Harrison model performed best among dual-parameter models. For ultra-tight Pc data, the error values in Table 4 indicate that Brooks and Corey, along with Thomeer, were the best-performing single-parameter models, while Skelt-Harrison and O'Meara Unimodal were superior among dual-parameter models. Table 4 also shows that the Bentsen and Anli model was the least accurate for both tight and ultra-tight Pc data sets, while the Brooks & Corey model was the most effective for these unconventional categories.

Table 4 Error in fit analysis

	J Function Model Name	*Error in Fit for All Pc Datasets*	*Error in Fit for Tight Pc Datasets*	*Error in Fit for Ultra-Tight Pc Datasets*
Models with one model-specific parameter	*Thomeer*	*6.26E-03*	*9.97E-03*	*2.89E-02*
	Brooks and Corey	*8.91E-03*	*8.64E-03*	*2.91E-02*
	Bentsen and Anli	*1.49E-02*	*1.21E-02*	*2.95E-02*
Models with two model-specific parameters	*Skelt-Harrison*	*6.68E-03*	*7.86E-03*	*2.87E-02*
	O´Meara Unimodal	*7.09E-03*	*8.49E-03*	*2.86E-02*

2.2.1. Evaluation of the Brooks & Corey Model

The results demonstrated that the Brooks & Corey model effectively fits both tight and ultra-tight data sets. The evaluation of five distinct J models was conducted for Pc data sets for tight formations (0.001 md < K < 0.1 md) and Pc data sets for ultra-tight (K < 0.001 md), as described in Section 5.2. A range of data sets from these categories was analyzed. For each data set, the Brooks and Corey model was applied to ascertain the typical λ characteristic of these unconventional data sets. The findings showed that the Brooks & Corey model accurately represents both tight and ultra-tight data sets.

Table 5 The λ analysis

Sample data set name	*Permeability, md*	*Porosity %*	*λ*	*Jd*	*Error in fit*
A-IPE-HG-195	0.0086	11.8	1.080	0.0540	2.06E-03
A-IPE-HG-120	0.00062	5.5	0.462	0.0326	3.23E-05
A-IPE-HG-141	0.0011	12.8	1.062	0.0228	8.80E-04
A-IPE-HG-142	0.0062	7.3	1.042	0.0377	1.40E-03
A-IPE-HG-112	0.008	10.5	1.179	0.0546	2.01E-04
A-IPE-HG-114	0.00957	10.2	1.497	0.0703	8.60E-04
A-IPE-HG-128	0.0199	12	0.458	0.0555	4.63E-04
A-IPE-HG-168	0.0364	9	0.613	0.0776	5.50E-04
A-IPE-HG-77	0.0416	9.5	0.386	0.0345	7.41E-04
A-IPE-HG-76	0.0512	9.8	0.492	0.0394	5.18E-04
A-IPE-HG-60	0.067	15.4	0.565	0.0827	2.79E-04
A-IPE-HG-101	0.0728	14.1	0.575	0.1242	3.16E-04
A-IPE-HG-167	0.0978	9.8	0.743	0.1016	1.99E-04
A-IPE-HG-9	0.137	11.4	0.556	0.0492	3.63E-04
A-IPE-HG-14	0.00016	3	0.670	0.0550	1.99E-04
A-IPE-HG-34	0.00025	4.5	0.766	0.0079	5.04E-04
A-IPE-HG-130	0.000064	8.2	0.694	0.0231	2.84E-04
A-IPE-HG-52	0.000343	5.5	0.704	0.0489	4.46E-05
A-IPE-HG-132	0.00028	4.2	0.951	0.0875	4.00E-03
A-IPE-HG-137	0.000374	3.7	0.357	0.1016	1.36E-03
A-IPE-HG-19	0.00039	4.2	0.826	0.0560	7.43E-04
A-IPE-HG-93	0.00025	7.8	0.664	0.0348	7.17E-04
A-IPE-HG-27	0.00021	4.3	0.487	0.0173	5.43E-04
A-IPE-HG-31	0.00034	5.7	0.475	0.0493	7.57E-06
A-IPE-HG-110	0.00117	8.4	0.513	0.0341	7.42E-04

Table 5 displays a selection of the evaluated data, detailing the sample data set names, K, φ, estimated λ, J-function displacement, and curve fitting error metrics. The estimated λ for these samples span from 0.313 to 1.49. To demonstrate the high correlation between the Brooks & Corey model and observed data, two specific sample data sets were chosen: a tight and an ultra-tight data set.

A data point from the tight data group, has a permeability (K) of 0.0086 md and a porosity of 11.8%, with an error in fit of 2.06E-3, indicating minimal deviation. Figure 4 illustrates a close match between the Brooks & Corey model fit and the actual data for this set, showing a λ of 1.08 and a J-function displacement of 0.054. The ultra-tight sample, has a permeability (K) of 0.00016 md and a porosity of 3%, with an error in fit of 1.99E-4, suggesting an excellent fit. Figure 5 illustrates an almost exact alignment between the Brooks & Corey model fit and the observed data, characterised by a λ of 0.67 and a J-function displacement value of 0.055.

2.2.2. Concave down effect

Certain Pc (or Leverett J) curves exhibit a concave-down section where dead volume errors become evident when the apparent Pc displacement, or the related displacement value in the J-function, is noted at a wetting phase saturation below 1. Figure 6 highlights this dead volume error in a dataset. Between wetting phase saturations of 1 and 0.97, some data points indicate that the non-wetting phase can more readily penetrate the rock. However, when the J-function value exceeds 0.04, the curve characteristics shift, making it harder for the non-wetting phase to enter. At this threshold, a discontinuity or change in curve shape occurs, which the Brooks and Corey model cannot capture, linking it to dead volume errors in Pc measurements. Hence, this effect should be adjusted to avoid being mistakenly interpreted as a change in rock characteristics, as illustrated in Figure 7.

In Pc studies, dead volume is defined as the quantity of fluid (such as mercury) that is presumed to fill the core sample but is, in reality, retained within the core holder or has penetrated surface vugs or irregular features. According to Shafer and Neasham (2000), this adjustment is known as the closure correction. In case dead volume is identified, it is essential to modify the experimental data, as it fails to reflect the genuine capillary characteristics of the core sample.

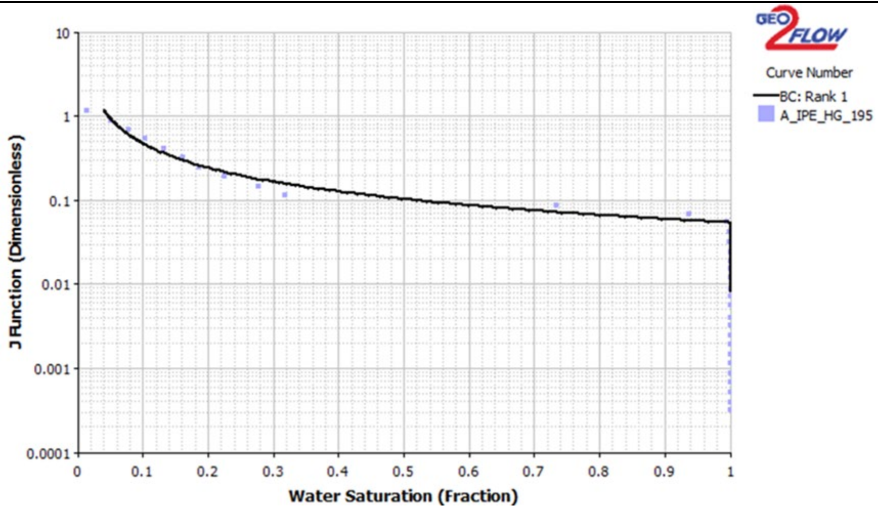

Figure 4 Comparison of actual and matched J-functions against Sw for a Pc sample dataset from tight sets

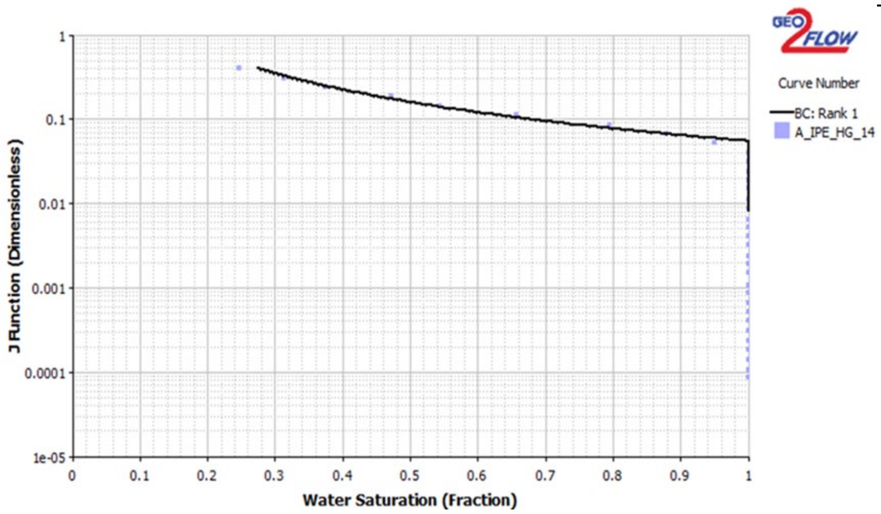

Figure 5 Comparison of actual and predicted J-functions against Sw levels for the Pc sample dataset from ultra-tight formations.

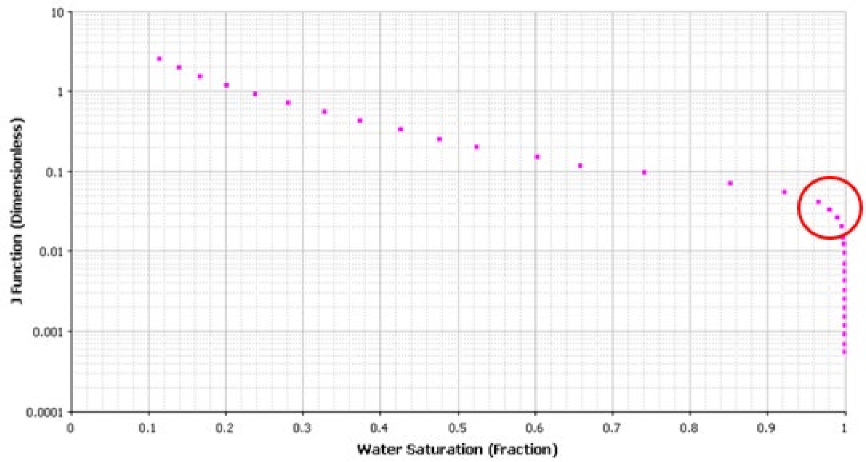

Figure 6 A Pc sample dataset with the dead volume error

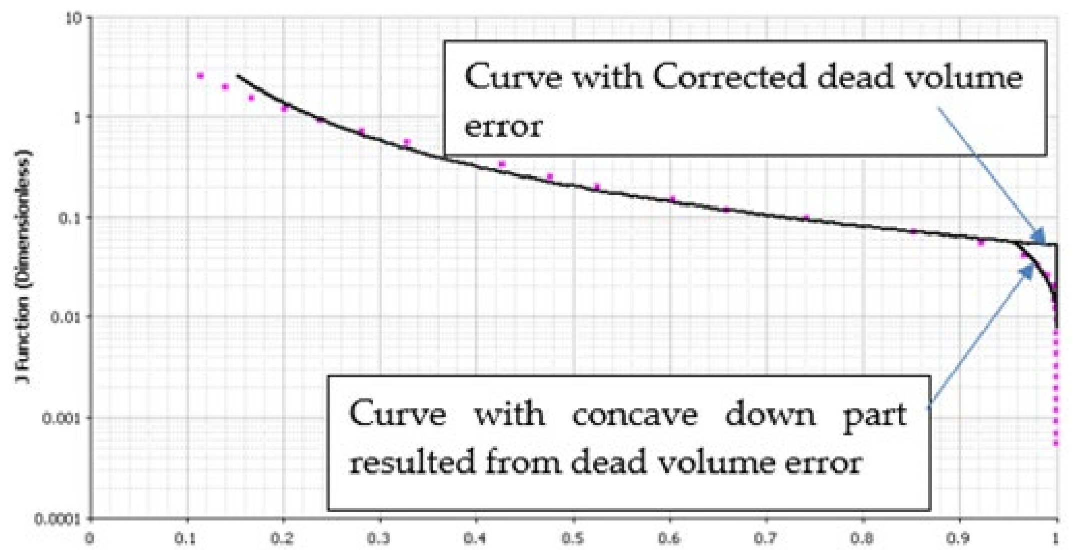

Figure 7 A Pc data sample adjusted for dead volume errors.

These observations indicated that the Brooks & Corey model, with its single specific parameter, provided a simple yet accurate representation of Pc data in unconventional rocks. It's important to note that these findings were derived from core samples from basins in the western US, reflecting a specific range of properties. Furthermore, the findings of this research indicate that to effectively characterise the behaviours of unconventional tight and ultra-tight rocks, the λ needs to be limited to a range of 0.3 to 1.5.Previously, a broader index range (from 1 to 4) was applied in the MFHW cleanup study, which requires adjustment to align with the findings presented in the following sections.

2.3. *Development, Modifying, and Validating the Model*

The MFHW Model was established using ECLIPSE 100 [52] to study the cleanup operation in multiple fractured horizontal wells. The equations and underlying physics utilised in Eclipse are thoroughly explained elsewhere [52] .Seven fractures were added to the 600 m long horizontal well in the new pre-fractured MFHW Model. Instead of using global refinement around fractures, MFHWs were built using local grid refinement (LGR). Using LGR allowed the authors to capture, with minimal CPU time increase, the impact of changing flow parameters in the SRV. The model's initial pressure is 7500 psi, and the average matrix porosity is 15%. The dimensions of the numerical models are shown in Table 1. The model is shown in Figure 8. The set numbers denote the sequence in which they were performed as a subset of a much larger set of simulations, not all included in this article. During the post-fracturing stage of the numerical modeling, controlled bottom-hole flowing pressure was applied to produce both gas and fracturing fluid (FF), which was found to be water. As shown in Figure 8, the fracture half-length is 90 metres as mentioned in Table 1.

For FF, the relevant compressibility and viscosity were calculated as 0.000005 (1/psia) and 0.5 cp, respectively. In the MFHW scenario's presumed base reference sets, the FF injected during the hydraulic fracturing stage was twice the volume of the fracture. It is important to note that a two-day period of well shut-in applied immediately after the FF injection and before the flowback production. The method of validating the amended VW model and its governing equations was previously discussed [30]. To validate the MFHW model, the well pressures vs production time estimated by simulation were compared to what was observed in an analytical model for MFHW [29].

Figure 9 compares the predicted well bottom-hole pressure (Pwf) by the simulation model with the analytical model as a function of production time. The fact that the two curves overlap and are stacked on top of one another supports the accuracy of the simulation model. It should be emphasised that this study takes into account twelve pertinent variables that have an impact on the post-fracturing cleanup processes. The first eight values among the twelve parameters represent the exponents and endpoints of the Brooks-Corey relationship for Kr in two separate phases.

The matrix's Pc is influenced by Km, IFT, and λ (pore size distribution index). The final variable is Kf .Table 2 lists the possible variation ranges of the parameters. It should be noted that six of the parameters given in Table 2—namely, DP, porosity of the matrix, and Swc and Sgc in both the fracture and matrix—are taken into consideration constants throughout a simulation set.

Equations 1 and 2 depict the capillary and threshold (entry) pressure, respectively [50,53]. Equations 3 and 4 establish the relationship between gas and water relative permeability, as formulated by Brooks and Corey in 1966. It is important to note that data is generated using either FFS or LHS sampling techniques for each simulation set, drawing from the specified parameter ranges listed in Table 2.

$$\frac{Pd}{IFT} = 0.0075 \times K^{-0.5} \tag{9}$$

- Interfacial tension (IFT)
- Km measured in mD

$$\left(\frac{Pd}{Pc}\right)^{\lambda} = \frac{Sw - Swr}{1 - Swr} \tag{10}$$

$$k_{rw} = K_{\max w} \times \left(\frac{Sw - Swr}{1 - Swr - Sgr}\right)^{nw} \tag{11}$$

$$k_{rg} = K_{\max g} \times \left(\frac{Sg - Sgr}{1 - Swr - Sgr}\right)^{ng} \tag{12}$$

Table 3 shows various simulation sets for each DP to fully understand how pressure drop (DP) affects the cleanup performance. The 12 relevant parameters in this study are scaled between 0 and 1, where 0 represents the lower bound and 1 represents upper limit, making the assesment of the cleanup processes via the response surface approach more effective (RSM).

2.4. The main output and RSM

Gas Production Loss (GPL), expressed as a percentage, measures the effectiveness of the cleanup process. It is determined by calculating the difference in cumulative fracture productions between a clean, undamaged fracture and an unclean, damaged fracture, and comparing it to the cumulative fracture productions of a clean, undamaged fracture.

$$\mathrm{GPL} = 100 \times \left[\frac{\mathrm{FGPT_{clean}} - \mathrm{FGPT_{unclean}}}{\mathrm{FGPT_{clean}}}\right] \tag{13}$$

FGPT: Field gas cumulative production

After a hydraulic fracturing operation, having a clean (undamaged) fracture is extremely difficult or technically impossible. In order to attain a much cleaner fracture and higher productivity, the current field tactics for fracturing operations could benefit from additional enhancements. This would require a comprehensive understanding of the parameters involved and their effects on post-fracturing activities. To facilitate comparison between different instances, the response parameter of GPL should be reported in a normalised format. The present work uses tornado charts to illustrate how the 12 previously listed characteristics affect gas production loss. According to this technique, if a parameter positively affects cleanup effectiveness, it reduces gas production loss (GPL) or increases the total amount of gas produced while the parameter is increased. In contrast, if a parameter harms cleanup effectiveness, it will result in a GPL or less cumulative gas production as its value increases. Response surface methodology is frequently used to examine how sensitive several relevant parameters are to a specific major output. RSMs in statistics and mathematics uncover a true relationship between multiple independent variables, such as x1, x2, x3, x4,..., xn, and the primary output (y or f(xi)).

Equation 6 defines the RSM, often the polynomial that best fits the data.

$$y = a_0 + \sum_{k=1}^{n} a_k x_k + \sum_{i=1}^{n} \sum_{j=i+1}^{n} a_i a_j x_i x_j + \sum_{l=1}^{n} a_l x_l^2 \quad (14)$$

Equation 6 lists four distinct RSM models:

- LRSM (Model for Linear Response Surface) with (a_0) and ($a_k x_k$).
- If (a_0) and ($a_k x_k$) are taken into account in addition to ($a_i a_j x_i x_j$), then LRSM with interaction (ILRSM) will be used.
- A pure quadratic response surface model (PQRSM) that takes into account the quadratic terms (a_0), ($a_k x_k$), and ($a_l x_l^2$).
- The Full Quadratic Response Surface Model (FQRSM) takes this into ($a_l x_l^2$).

This study determined GPL as a function of those 12 pertinent factors for the Latin hypercube sampling (LHS) approach using ILRSM and FQRSM models. A Python code was created to perform every simulation in a simulation set, including the pre-and post-processing stages of the fracturing procedure.

2.5. The second response surtface model

During the flowback, some of the injected fracture fluid (FF) returns as flowback. The FF volume that returns can vary greatly depending on key parameters and the design of the fracture. The FF that is produced normally includes a combination of surface-returned FF, some formation brine, and a portion of the injected chemicals. Consequently, understanding the volume of produced water is critical. Managing the produced FF poses a significant challenge in the development and production of unconventional gas formations due to strict regulations concerning FF flowback, its environmental impact, and limited disposal options. These factors push operators to constantly review and adjust their hydraulic fracturing strategies and FF flowback management approaches. To address this, a new dimensionless term, Produced Fracture Fluid (PFF), was established. The influence of key parameters, similar to those affecting GPL, on PFF has been examined. PFF, which serves as the second response metric, indicates the proportion of flowback relative to the total injected FF during the fracturing process, determined by the following equation.

$$PFF = 100 \times \left[\frac{The\ volume\ of\ produced\ FF\ or\ simply\ Field\ water\ production}{Total\ FF\ injected\ at\ fracturing\ stage(FF\ injection\ stage)}\right] \quad (15)$$

2.6. Analysis Methodology

This study examines five distinct sets of MFHWs (each set consists of 1000 simulation runs). Table 3 lists each of those various sets in total. The fact that each set has a reservoir with identical dimensions should be emphasised. However, each set has a different Pc pertinent parameter (i.e., Λ), different pressure drawdown, matrix permeability, and FF injection volume. The 12 pertinent factors are considered by the base reference set, with the default ranges displayed in the table. When a parameter in Table 3 has a tick next to it, the parameter's default variation range is considered; else, a new range of variation is established, and the name of the new sets is determined based on the degree of dissimilarity between a range of parameter values and a the set that was selected as reference.

3. Results and Analyses

The previous and updated pore size distribution ranges relevant to Pc for unconventional formations with varying Kmr, DP, and FVR were utilized. This approach aimed to assess how these parameters influence cleanup efficiency when employing unconventional Pc. The resulting data were examined, compared, and discussed in this section

3.1. Unconventional capillary pressure

Two sets have been implemented and analysed in this section. Set 8 base reference set where the dimensions and parameters variation range were shown in Tables 1& 2. As mentioned previously, the MFHW is shown in Figure 8.

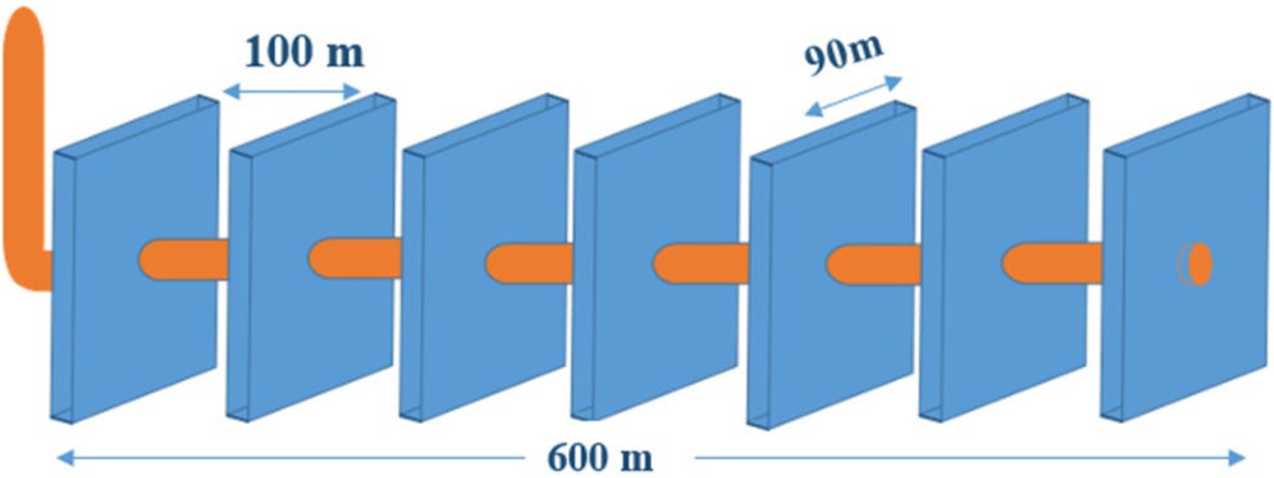

Figure 8 The modelled MFHW

The updated λ range which corresponds to the Pc values for tight/ultra-tight formations, is also used in Set 30 (0.3<λ< 1.5),. Importantly, all parameters and dimensions align with those of set 8, apart from the revised λ range. A comparison was made between the GPL tornado chart for set 30, featuring the new λ range (0.3<λ< 1.5, Figure 10), and the set 26 Base Reference set (Figure 9). The comparison showed consistent trends across both charts for all key parameters. Additionally, it was noted that in set 30, with its lower λ range, Pc-related parameters, particularly Λ, have a greater influence on GPL. This increased influence is attributed to the narrower λ range in set 30, which enhances the importance of Pc values relative to set 26.

$$K_m \downarrow, \quad IFT \uparrow, \quad \lambda \downarrow, \quad S_w \downarrow \rightarrow P_c \uparrow$$

The effect of fluid mobility, particularly water mobility, within the matrix is slightly more pronounced in set 30 contrasted to set 26, which has lower Pc values. This difference arises from the higher Pc in the matrix of set 30, which hinder fluid mobility.

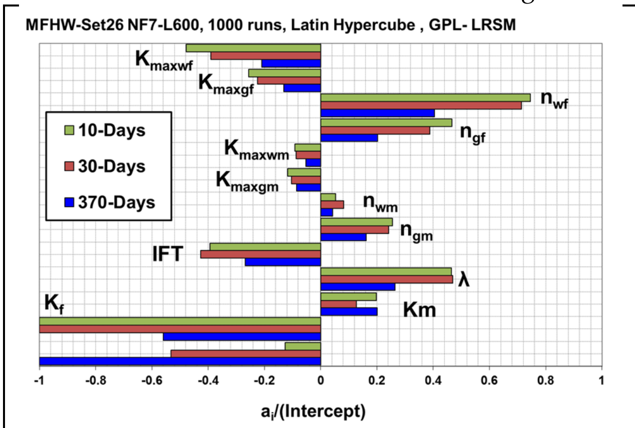

Figure 9 GPL Tornado chart of the Base Reference set.

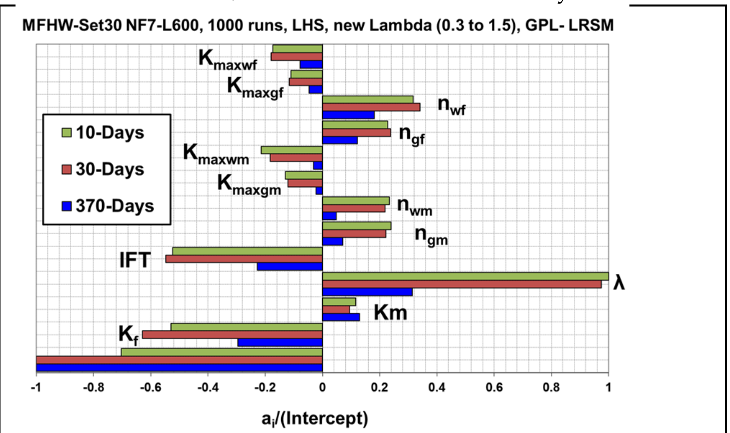

Figure 10 GPL Tornado chart of the effect of unconventional Pc

The tornado chart for PFF relating to set 30, utilising the updated λ range of 0.3 to 1.5 as shown in Figure 12, was in comparison to the chart for the Set 26 Base Reference set that included a modified λ range (Figure 11). Both charts demonstrated a consistent trend across all key parameters exclusive of Kf: in Set 30, an increase in Kf led to a decrease in FF production (PFF), whereas the reverse effect was observed in Set 26. A new MATLAB code was developed, and water saturation (Swat) as well as values from the GRDECL file in Floviz at the end of the soaking period were extracted and utilized. In Eclipse simulation, a GRDECL file defines the grid structure and geometry, including grid dimensions, coordinates, and properties. It is essential for setting up the simulation as it provides the spatial framework for the reservoir model.

To further investigate the observed shift in the Kf trend shown in the PFF tornado chart for Set 30, run number 29 was chosen, where Kf was set close to its maximum value. A Sw map was then created to visualize water distribution at the end of the soaking period for this high-Kf scenario and to contrast it with the minimum-Kf scenario, in which Kf was set to its lowest value.

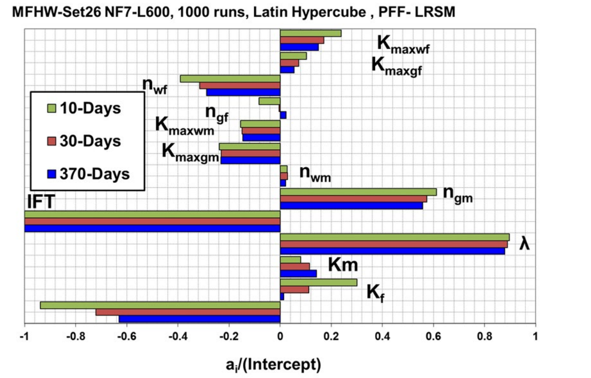

Figure 11 PFF Tornado of the Base Reference set.

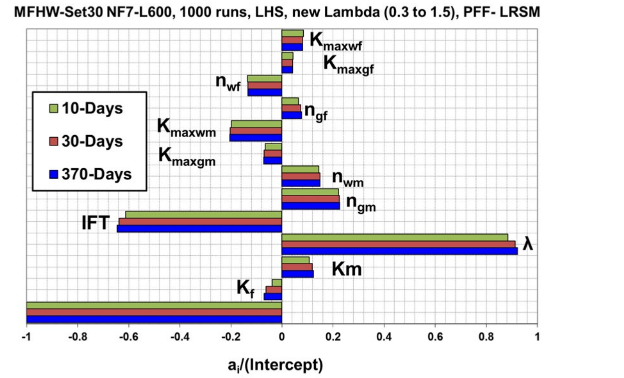

Figure 12 PFF Tornado chart of the effect of unconventional Pc

Examining Figures 13, 14, and 15 highlights significant contrasts between the Max-Kf and Min-Kf scenarios. In the Max-Kf scenario (Figure 13), a specific zone (Region B) within the first 45 meters of the fracture's half-length from the well exhibits water saturation levels between 30% and 70%. Conversely, in the Min-Kf scenario (Figure 14), a considerable amount of fracturing fluid (FF) is either injected into or absorbed by the matrix, resulting in water saturation levels ranging from 60% to 100% (Region A) within approximately the initial 10 meters of the fracture near the well. This disparity occurs because, during FF injection, the fluid moves significantly faster and more freely through the fracture in the Max-Kf scenario compared to the Min-Kf case. This resulted in a more dispersed FF distribution, particularly within the matrix, in the Max-Kf scenario. Therefore, in the case with Min-Kf, large volume of FF is infused or imbibed within a smaller matrix distance near the fracture (around 10 m), creating Region A, which has higher water saturation (Sw) and lower capillary pressure (Pc). This region is more easily replicated during the backflow phase than in the Max-Kf scenario.

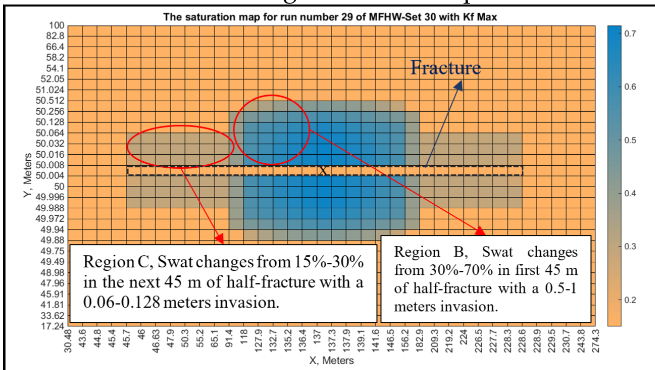

Figure 13 FF saturation distribution map for run No. 29, with Kf-max of Set 30 following a shut-in period

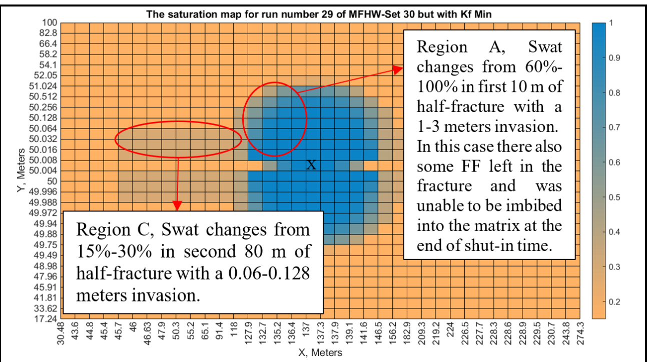

Figure 14 FF saturation distribution map for run No. 29, with Kf-min of Set 30 following a shut-in

Pc is plotted in Figure 15 for Sets 26 and 30 (run No: 29) with different areas indicated in Figures 13 and 14. From Figure 15, it is evident that Set 30 generally displays significantly higher Pc values compared to Set 26. This difference is due to the narrower λ range in Set 30 (0.3 to 1.5) compared to Set 26 (1 to 4), leading to an increase in Pc. Additionally, for Set 30, the Pc curve remains identical for both Kf-Max and Kf-Min.

In Region A, where water saturation ranges from 60% to 100%, the capillary pressure (Pc) spans from 100 psi to 20 psi for Set 30, and from 30 psi to 20 psi for Set 26. In Region B, with Sw levels between 30% and 70%, Pc fluctuates between 2100 psi and 60 psi for Set 30, and between 80 psi and 25 psi for Set 26. Lastly, in Region C, where water saturation is between 0% and 30%, Pc decreases from infinity to 2100 psi for Set 30, and from infinity to 80 psi for Set 26.

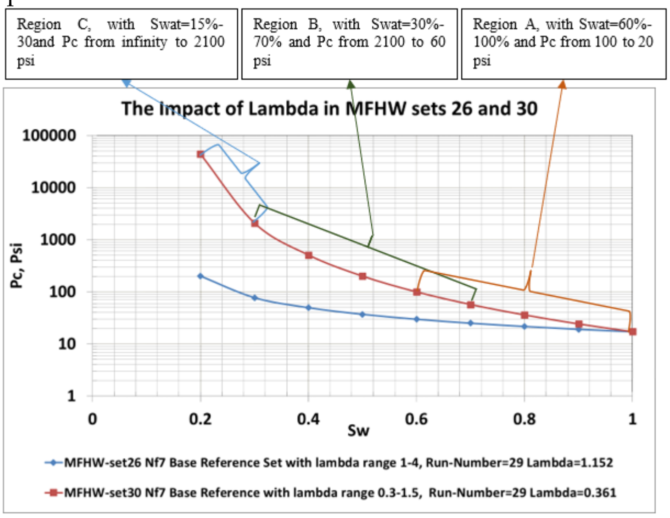

Figure 15 Pc along with the various regions discussed, is illustrated in Figures 14 and 13

Notably, Regions A, B, and C each exhibit distinct Pc values. Through the Flowback period, a rise in FF production is noted, attributed to elevated Sw values and a reduced Pc, which signifies a decrease in retained FF within the set featuring the lowest Kf. This explains the negative Kf value displayed in the associated tornado chart (Figure 12).

Kf influences FF production in two distinct ways:

1. As the value of the Kf increases, the mobility within the fracture of the FF increases during the production stage necessary for increased production of the FF.
2. Higher Kf increases the FF fracture mobility during the injection phase leading to improved distribution of the FF and reduced Sw values in the matrix and hence higher Pc values that hold additional FF during the production phase hence less FF output.

In Set 30, the second influence of Kf was notably dominant, resulting in a shift in the trend of Kf in the PFF tornado chart for this set, as shown in Figure 12. Additionally, for Set 30, where the λ range varies from 0.3 to 1.5, the parameters related to Pc, especially Λ, had the highest impact on GPL.This is because the λ range of set 27 is much narrower as compared to set 26 and therefore the Pc values are much more sensitive.

An additional key observation in the PFF tornado charts for Sets 26 and 30 (Figures 12 and 13) is the inverse relationship between FF production and water mobility within the matrix. This is due to the dual effects of matrix water mobility on FF production:

1. 1. Maximum Kmaxwm and minimum nwm reduces the extent of water bound with the matrix and increases the mobility of FF within the matrix during the period of production leading to higher production of FF.
2. 2. The maximum Kmaxwm and minimum nwm also enhance the distribution of FF throughout the matrix during the injection phase with better distribution of FF throughout the matrix, lower Sw in the matrix and thus higher Pc values. These elevated Pc values keep a greater amount of FF through the manufacturing process, consequently lowering FF creation.

As shown in Figure 16, stronger Pc values in Set 30 correspond to lower FF production, consistent with the fact that higher Pc values preserve FF more effectively, reducing FF flowback. Figure 17 plots GPL, PFF, and cumulative gas to water production proportion (i.e., FGPT/FWPT) for various runs in Set 30, while Figure 18 illustrates that increased FF production results in higher GPL. This aligns with previous observations in sets with Kmr=1, where retained FF within the matrix corresponds with reduced GPL values.

Investigating these two sets with two approaches toward estimating Pc highlights that employing IFT reduction chemicals will increase GPL in sets with tight sand formation.

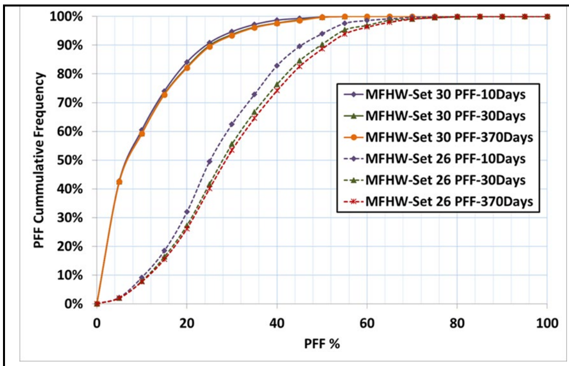

Figure 16 PFF Histogram chart of unconventional Pc

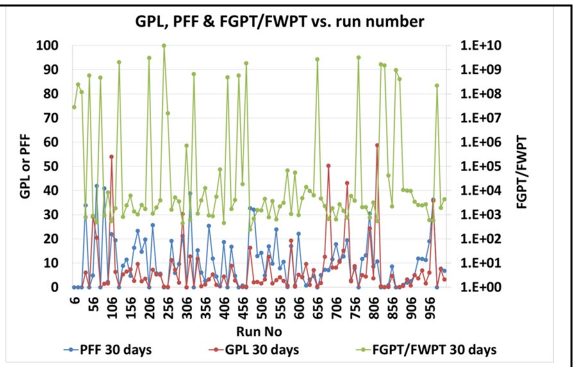

Figure 17 Impact water retention and flowback on Gas production

3.2. Sets featuring various Kmr, FVR, and DP configurations.

Therefore, to compare the cleanup efficiency under those unconventional Pc conditions, three additional sets were conducted with Kmr=100, significantly increased FVR, and high DP. The idea was to assess the impact of the given parameters on cleanup efficacy bearing in mind unconventional Pc. Its extension was not incorporated into the subsequent analysis of unconventional Pc because the results obtained from the analysis of the SFVW and MFVW sets indicated that extensive ST further enhances FF penetration within the matrix, thus enhancing FF saturation at the same time reducing the FF flowback. That, however, appears to be applicable only to the early stages of the production process.

3.3. Low Km sets with unconventional Pc

This Set was implemented in order to investigate the impact of a remarkably low Km scale (Kmr=100) on cleanup efficiency under rather untypical Pc conditions. The Km variation range was cut down from 1mD-100 mD in Set 30 to a new range of 0.01mD - 1 mD in this set. In the analysis of the GPL tornado charts for Set 31 as a comparison to the highly compact formation with that presented in Figure 19 and the Set 30 Base Reference set in Figure 11 that used a different Km range, most of the key parameters had a similar trend except for the Km factor. In Set 30, change in Km was seen to change GPL, with Km being significantly effective on Pc as depicted in figure 10. However, in the case of Set 31, there is negative relationship between Km and GPL showing an increased value of Km decreases GPL with importance of Km to mobility. This shift is attributed to the low permeability characteristic of the rock in this set which greatly limits the mobility of fluids. The mobility of fluids within the matrix is more critical here than in Set 30 as previously discussed The impact of mobility of the fluids becomes very important following the already high values of Pc. It can be noted in figures 18 and 20; the GPL and PFF histograms of the two sets show that the degree of cleanup outcomes are almost similar, due to the excessive Pc values.

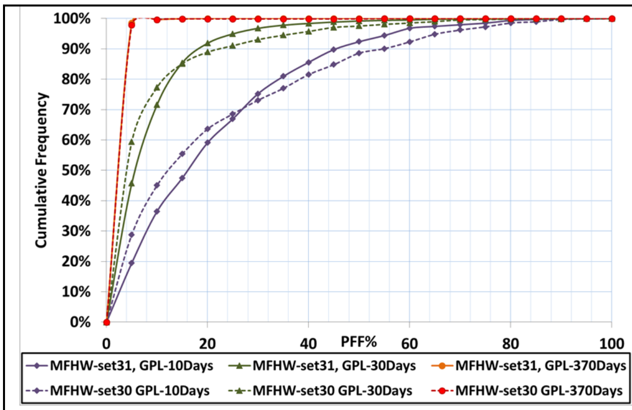

Figure 18 GPL Histogram chart of the effect of ultratight formations

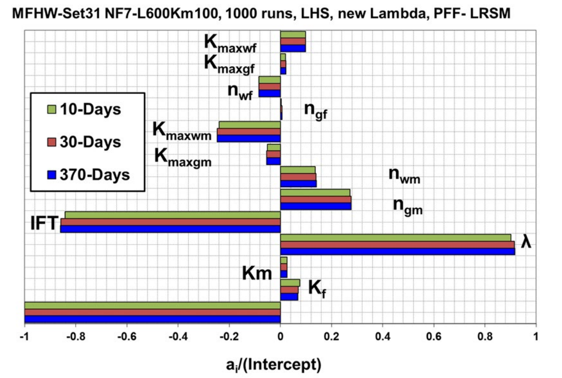

Figure 19 PFF Tornado chart of the effect of ultratight formations

When the PFF chart of ultra-tight Set 31 is compared to the chart of Set 30 Base Reference set, all the factors described in the tornado chart of Figure 19 except Kf are similar to that of Figure 12. In Set 31 Kf primary effect is higher while in Set 30 wherein the secondary effect of Kf is considered.

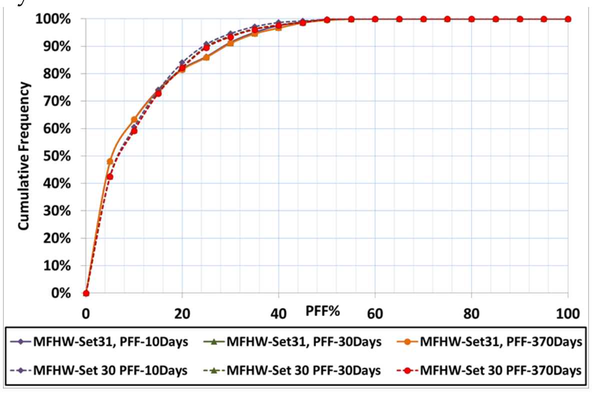

Figure 20 PFF Histogram chart of the effect of tightness

A comparison of the sets of unconventional formations highlights that employing IFT reduction chemicals will increase GPL in sets with tight sand formation (with Km variation ranges of 1 μD-100 μD and 0.1 μD-10 μD). In contrast, employing such substances to decrease Pc and subsequently lessen GPL in ultratight plays (i.e., km range of 0.01 μD-1 μD) is advised. In essence, it has been established that incorporating IFT (interfacial tension) reducing agents into fracturing fluids is not advisable in tight formations due to its adverse effect on gas production. However, ultratight formations benefit greatly from it since it increases the gas rate.

3.4. Higher FF volume sets with unconventional Pc

This Set was done to determine the effect of enhancing the FVR from 2 in Set 30 to 10 on cleanup efficiency under unconventional Pc condition. When comparing the GPL tornado chart for the Set 32 with FVR=10 (Figure 21) with the Set 30 Base Reference set (Figure 10) which incorporates adjustments to FF injection in the injection phase, similar trends were observed for all the corresponding parameters on both charts. Furthermore, the following observations were made:

1. In this set, the impact of fluid mobility within the matrix and fracture on GPL was more notable related to the base reference set.
2. The absolute values of all 12 relevant parameters at one year of production were still high; it means that the cleanup process is significantly longer (up to a year) compared to the duration set by MFHW, as 30.

These are due to the fact that the total FF volume introduced in this set is greatly larger. Figure 22 also displays that the cleanup task of the high FVR configuration takes a longer time. From Figure 23 the PFF tornado chart considering the data in Set 32, it can be observed that the initial change influenced the Kf on the FF production predominantly.

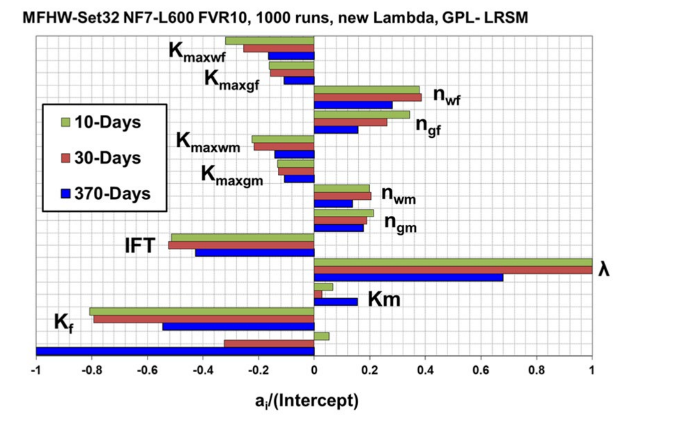

Figure 21 GPL Tornado chart of the effect of FF volume

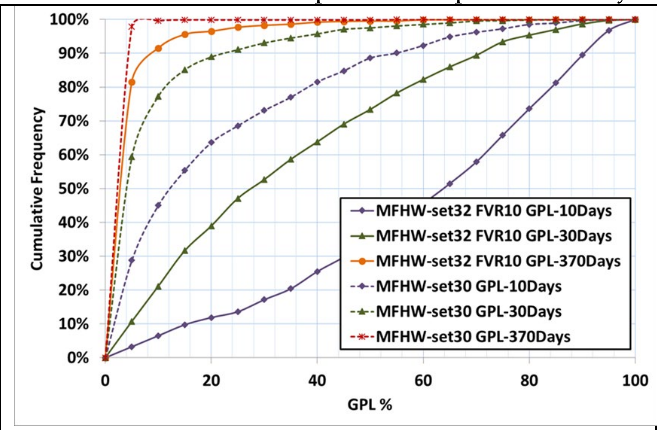

Figure 22 GPL Histogram chart of the effect of FF volume

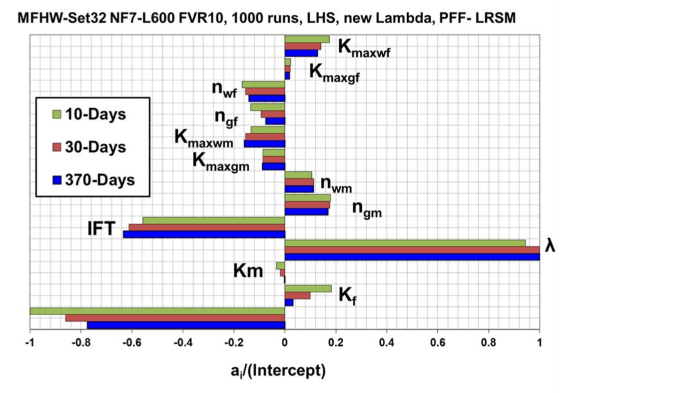

Figure 23 PFF Tornado chart of the effect of FF volume

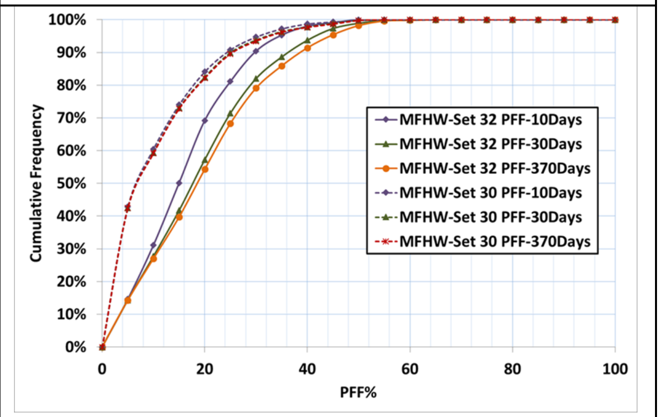

Figure 24 PFF Histogram chart of the effect of FF volume

Figure 24 provides the histogram of the PFF for the, Set 30 (FVR=2) and Set 32 (FVR=10). Notably, the cumulative frequency curves of Set 32 at the three production stages concerns not overlay one on another, unlike the Set 30 results suggesting FF manufacturing goes on until one year.

3.5. Impact of increased pressure drawdon and unconventional Pc

This Set was performed to capture the effect of DP increase, with new Pc, on the cleanup efficiency (DP was raised from 1000 in Set 30 to 4000 in this set). Using the GPL tornado chart of the Set 33 (DP=4000, Figure 25) with the GPL tornado chart of the Set 30 Base Reference set (Figure 10)–all the significant parameters showed the same trend as the DP was changed from the earlier value. Notably, the impact of Λ, IFT, and Km on cumulative gas loss was marginally less pronounced in Set 33 compared to Set 30, due to the increased viscous force , i.e., higher DP, which made it more challenging to retain FF within the matrix. The influence of Kf on FF flowback was minimal given the high DP applied in this set (Figure 29).

Figures 26 and 28 indicate that larger DP didn't expedite the cleanup process in this configuration with unconventional capillary pressure model. While higher DP typically enhances cleanup efficiency in the fracture and adjacent matrix, Furthermore, it raises the rate of FF flowback from more away from the fracture and from inside the matrix at greater depths, which is not beneficial in terms of cleanup. This amplified FF flowback is illustrated in Figure 28. The balancing effect of these two opposing influences resulted in nearly identical cleanup performance across both sets.

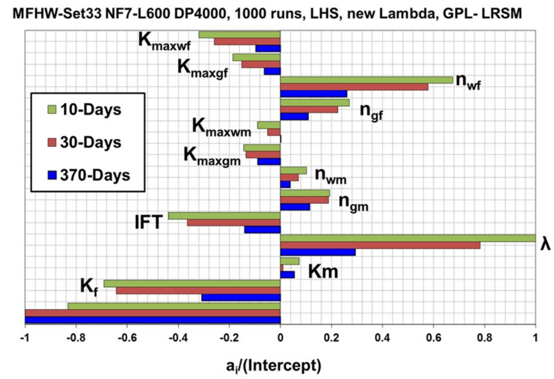

Figure 25 GPL Tornado chart showing the impact of pressure drawdown

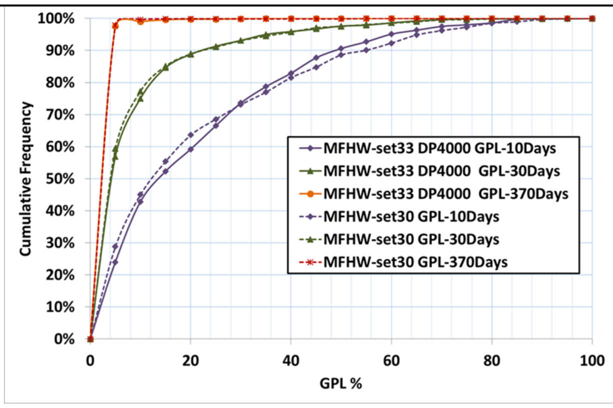

Figure 26 GPL Histogram chart showing the impact of pressure drawdown

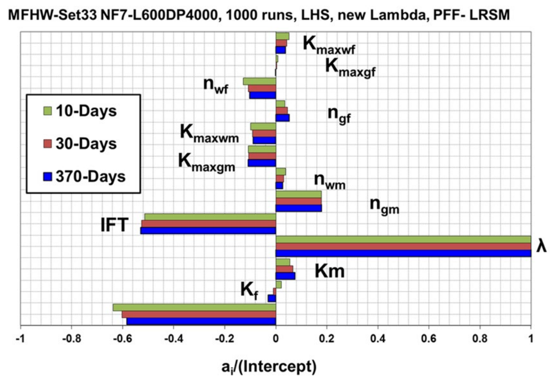

Figure 27 PFF Tornado chart showing the impact of pressure drawdown

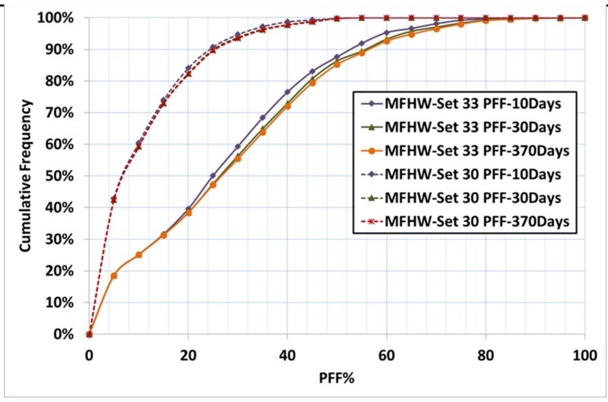

Figure 28 PFF Histogram showing the impact of pressure drawdown

4. Conclusions

This work aims to enhance the recent comprehension of HF treatments for practical field usage by building upon previous research conducted by Nasriani et al. (2018), Nasriani and Jamiolahmady (2018a and b), and Nasriani and Jamiolahmady (2019). The present study seeks to investigate the effect of unconventional Pc on the cleanup effectiveness of MFHWs. For this reason, an assessment of the Pc correlations presented in the current paper for tight and ultra-tight formations used the Geo2Flow software.

For these five sets, a new term, analogous to dimensionless GPL, was incorporated to depict the influence of the relevant parameters on the FF production—an aspect critical to the HF of unconventional reservoirs. Outlined below are the principal findings and conclusions of this work:

1. Analyses of the Pc models, based on 200 sets of conventional and unconventional Pc data, revealed that the Brooks and Corey model can be used as a simple, one-parameter Pc model that adequately describes the Pc data for nonconventional formations.
2. On this basis, this research suggests that the λ range should be limited to the range of 0.3-1.5 for a better characterisation of uncon-ventional tight and ultra-tight rocks. These changes were integrated into the model to reflect the unconventional Pc in the new range indicated below.
3. As mentioned earlier, this work found a concave-down section in a few Pc curves due to dead volume in Pc determination. Dead volume corrections are therefore important because these errors should not be confused with changes in the in-herent properties of the rock.
4. As expected, various Pc-related parameters, specifically Λ, were substantially affecting GPL in all the sets with Pc that was adjusted for unconventional cases, incorporated in the sets. This can be attributed to the difference in λ variation range identified

in the unconventional Pc sets, which caused the Pc more sensitive than in the conventional sets.

5. Kf influenced FF production in two distinct ways:
    - A higher Kf improved FF mobility within the fractured region during the production phase, leading to increased FF production.
    - Higher values of Kf also promoted increased FF mobility within the fracture region throughout the injection phase and also provided better distribution of FF in the fracture, lower saturation (Sw) in the matrix phase and higher Pc values. These higher Pc values maintained a greater proportion of FF during production and, thus, lower FF.
6. PFF tornado charts indicated a decline in FF production as water mobility within the matrix increased. This outcome is due to the dual impact of matrix water mobility on FF production:
    - More FF is produced during the production stage when there is greater matrix water mobility, which improves FF mobility inside the matrix.
    - Greater FF matrix mobility through the injection phase is a result of more substantial water mobility in the matrix; this leads to more dispersed FF, lower matrix Sw values, and higher Pc values. Higher Pc values produce less FF because they retain more FF during backflow.
7. When the same sets were exposed to the reduced Km or increased injected FF volume to FVR for the sets using unconventional Pc, the outcomes were similar to when the conventional Pc was used. The primary ones are:
    a. It was only after bringing down the Km range or up the FVR that the cleanup was significantly hampered.
    b. However, in the set with Kmr=1 , the Km coefficient was positive suggesting that an increase in Km raised GPL. This suggested that the Km effect which reduces the value of Pc and increases the output of FF was critical. In the set with Kmr = 100 the Km coefficient was negative, therefore the increase of Km leads to the decline of GPL. This implied that the Km actually had a great influence on the mobility of the business. The cause of this change in trend is that the rock in this set is very consolidated, and thus makes matrix fluid movement practically impossible.
    c. These are asymptotic and numerical values illustrating the impact of fluid mobility on GPL at the set with a higher FVR than at the set with lower FVR.
8. As mentioned before, the cleanup process in the Set with atypical PC was not accelerated by the augmentation of DP. This is because, as as described earlier, while increasing DP accelerates the cleanup in the fracture and its vicinity the matrix surrounding the fracture and at some distance away from the fracture repairs faster and reduces flowback from deeper FF zones in the matrix. These two impacts tended to cancel each other out and the sets with standard and unusual Pc curves revealed cleaner output with comparable efficiency. The higher viscous force leads to a higher FF flowback in the relevant set, and that is why there is higher FF flowback in this current high DP set with atypical Pc. But the interaction of most of the FF flow back with conventional PC is found at a moderate value of DP.
    i. A stronger viscous force leads to the formation of more FF flowback in the relevant set, and that is why there is more FF flowback in this high DP set with executive pressure coefficient that deviates from the norm. However, since conventional Pc does not have as much significant Pc value as the unconventional Pc to continue to keep the FF inside the matrix, most of the flowback occurs at moderate values for DP.
9. A comparison of the sets of tight and ultratight formations highlights that employing IFT reduction chemicals will increase GPL in sets with tight sand formation (with Km variation ranges of 1 μD-100 μD and 0.1 μD-10 μD). In contrast, employing such

substances to decrease Pc and subsequently lessen GPL in ultratight plays (i.e., km range of 0.01 μD-1 μD) is advised. To put it differently, the study has established that incorporating IFT-reducing agents into fracturing fluids negatively impacts gas production rates in tight formations but is highly beneficial in ultratight formations as it increases production rates.

- The wastewater or flowback fluid that returns from the well is expected to have high concentrations of naturally occurring minerals and metals that have dissolved into the water from the shale and other rock formations.
- Additionally, a small amount of the non-hazardous chemicals injected during the fracturing process and naturally occurring radioactive material (NORM) may be present in the fluid. Therefore, this conclusion is environmentally significant. Consequently, it is strongly advised against using IFT-reducing agents in tight formations to aid the matrix in imbibing most of the FF and minimising flowback.

References

1. The U.S. Energy Information Administration (EIA) NATURAL GAS.
2. International Energy Agency, I. *Gas Market Report, Q3-2024*; 2024;
3. Energy Matters Enbridge Is Natural Gas Environmentally Friendly?
4. Campin, D. Environmental Regulation of Hydraulic Fracturing. **2015**, doi:10.2118/166146-PA.
5. Chen, B.; Barboza, B.R.; Sun, Y.; Bai, J.; Thomas, H.R.; Dutko, M.; Cottrell, M.; Li, C. A Review of Hydraulic Fracturing Simulation. *Archives of Computational Methods in Engineering* **2021**, 1–58.
6. Yu, H.; Xu, W.; Li, B.; Huang, H.; Micheal, M.; Wang, Q.; Huang, M.; Meng, S.; Liu, H.; Wu, H. Hydraulic Fracturing and Enhanced Recovery in Shale Reservoirs: Theoretical Analysis to Engineering Applications. *Energy & Fuels* **2023**, *37*, 9956–9997.
7. Davoodi, S.; Al-Shargabi, M.; Wood, D.A.; Rukavishnikov, V.S. A Comprehensive Review of Beneficial Applications of Viscoelastic Surfactants in Wellbore Hydraulic Fracturing Fluids. *Fuel* **2023**, *338*, 127228.
8. Osiptsov, A.A. Fluid Mechanics of Hydraulic Fracturing: A Review. *J Pet Sci Eng* **2017**, *156*, 513–535.
9. Bennion, D.B.; Thomas, F.B.; Ma, T. Recent Advances in Laboratory Test Protocols to Evaluate Optimum Drilling, Completion and Stimulation Practices for Low Permeability Gas Reservoirs 2000.
10. Zhao, J.; Ren, L.; Jiang, T.; Hu, D.; Wu, L.; Wu, J.; Yin, C.; Li, Y.; Hu, Y.; Lin, R. Ten Years of Gas Shale Fracturing in China: Review and Prospect. *Natural Gas Industry B* **2022**, *9*, 158–175.
11. Bin, Y.; Mingze, Z.; Siwei, M.; Zhang, W.; Zheng, H. Intelligent Identification and Real-Time Warning Method of Diverse Complex Events in Horizontal Well Fracturing. *Petroleum Exploration and Development* **2023**, *50*, 1487–1496.
12. Qun, L.E.I.; Yun, X.U.; Bo, C.A.I.; Baoshan, G.; Xin, W.; Guoqiang, B.I.; Hui, L.I.; Shuai, L.I.; Bin, D.; Haifeng, F.U. Progress and Prospects of Horizontal Well Fracturing Technology for Shale Oil and Gas Reservoirs. *Petroleum Exploration and Development* **2022**, *49*, 191–199.
13. Nianyin, L.; Jiajie, Y.; Chao, W.; Suiwang, Z.; Xiangke, L.; Jia, K.; Yuan, W.; Yinhong, D. Fracturing Technology with Carbon Dioxide: A Review. *J Pet Sci Eng* **2021**, *205*, 108793.
14. Dong, Z.; Holditch, S.A.; McVay, D.; Ayers, W.B. Global Unconventional Gas Resource Assessments 2011.
15. Niu, W.; Sun, Y.; Zhang, X.; Lu, J.; Liu, H.; Li, Q.; Mu, Y. An Ensemble Transfer Learning Strategy for Production Prediction of Shale Gas Wells. *Energy* **2023**, *275*, 127443.
16. Guo, J.; Lu, Q.; He, Y. Key Issues and Explorations in Shale Gas Fracturing. *Natural Gas Industry B* **2023**, *10*, 183–197.

17. Shen, W.; Ma, T.; Zuo, L.; Yang, X.; Cai, J. Advances and Prospects of Supercritical CO2 for Shale Gas Extraction and Geological Sequestration in Gas Shale Reservoirs. *Energy & Fuels* **2024**, *38*, 789–805.
18. He, X.; Chen, G.; Wu, J.; Liu, Y.; Wu, S.; Zhang, J.; Zhang, X. Deep Shale Gas Exploration and Development in the Southern Sichuan Basin: New Progress and Challenges. *Natural Gas Industry B* **2023**, *10*, 32–43.
19. Niu, W.; Lu, J.; Sun, Y.; Liu, H.; Cao, X.; Zhan, H.; Zhang, J. A Review of the Application of Data-Driven Technology in Shale Gas Production Evaluation. *Energy Reports* **2023**, *10*, 213–227.
20. Li, H. Coordinated Development of Shale Gas Benefit Exploitation and Ecological Environmental Conservation in China: A Mini Review. *Front Ecol Evol* **2023**, *11*, 1232395.
21. Clark, J.B. A Hydraulic Process for Increasing the Productivity of Wells. *Journal of Petroleum Technology* **1949**, *1*, 1–8, doi:10.2118/949001-G.
22. Garrison, A.D. Treatment of Wells 1945.
23. Height, B.C. Process of Increasing Permeability of Sands and Strata 1944.
24. Lee, R.E. Method of Treating a Producing Formation 1939.
25. Holditch, S.A. Factors Affecting Water Blocking and Gas Flow From Hydraulically Fractured Gas Wells. **1979**, doi:10.2118/7561-PA.
26. Montgomery, K.T.; Holditch, S.A.; Berthelot, J.M. Effects of Fracture Fluid Invasion on Cleanup Behavior and Pressure Buildup Analysis. In Proceedings of the Proceedings - SPE Annual Technical Conference and Exhibition; 1990; Vol. Pi, pp. 279–290.
27. Pope, D.; Britt, L.K.; Constien, V.; Anderson, A.; Leung, L. Field Study of Guar Removal from Hydraulic Fractures. *SPE International Symposium on Formation Damage Control* **1996**, 1–7, doi:10.2118/31094-MS.
28. Gdanski, R.D.; Weaver, J.; Slabaugh, B.; Walters, H.; Parker, M. SPE 94649 Fracture Face Damage - It Matters. *Water (Basel)* **2005**.
29. Nasriani, H.R.; Jamiolahmady, M. Flowback Cleanup Mechanisms of Post-Hydraulic Fracturing in Unconventional Natural Gas Reservoirs. *J Nat Gas Sci Eng* **2019**, *66*, 316–342, doi:https://doi.org/10.1016/j.jngse.2019.04.006.
30. Nasriani, H.R.; Jamiolahmady, M. Maximizing Fracture Productivity in Unconventional Fields; Analysis of Post Hydraulic Fracturing Flowback Cleanup. *J Nat Gas Sci Eng* **2018**, *52*, doi:https://doi.org/10.1016/j.jngse.2018.01.045.
31. Tech-Flo Consulting Available online: http://www.tech-flo.net/frac-flowback.html.
32. Halliburton Available online: https://www.halliburton.com/en-US/ps/testing-subsea/reservoir-testing-analysis/calibr.html?node-id=i4msmulo.
33. Ghahri, P. Modelling of Gas-Condensate Flow around Horizontal and Deviated Wells and Cleanup Efficiency of Hydraulically Fractured Wells, Heriot-Watt University, 2010.
34. Nasriani, H.R.; Jamiolahmady, M. A Comparison of Clean-Up Efficiency of Multiple Fractured Horizontal Wells and Hydraulically Fractured Vertical Wells in Tight Gas Reservoirs. In Proceedings of the SPE Europec featured at 80th EAGE Conference and Exhibition; Society of Petroleum Engineers, June 11 2018.
35. Nasriani, H.R.; Jamiolahmady, M.; Alajmi, E. An Integrated Study of Cleanup Efficiency of Short Hydraulic Fractured Vertical Wells Using Response Surface Methodology. In Proceedings of the 76th EAGE Conference and Exhibition 2014.; 2014.
36. Nasriani, H.R.; Jamiolahmady, M.; Saif, T.; Sánchez, J. A Systematic Investigation into the Flowback Cleanup of Hydraulic-Fractured Wells in Unconventional Gas Plays. *Int J Coal Geol* **2018**, *193*, doi:10.1016/j.coal.2018.04.012.

37. Nasriani, H.R.; Jamiolahmady, M.; Alajmi, E.; Ghahri, P. A Study of Hydraulic Fracturing Clean-up Efficiency in Unconventional Gas Reservoirs Using Statistical Approaches. In Proceedings of the ECMOR XIV-14th European Conference on the Mathematics of Oil Recovery; 2014.
38. Nasriani, H.R.; Borazjani, A.A.; Iraji, B.; MoradiDowlatAbad, M. Investigation into the Effect of Capillary Number on Productivity of a Lean Gas Condensate Reservoir. *J Pet Sci Eng* **2015**, *135*, 384–390, doi:10.1016/j.petrol.2015.09.030.
39. Nasriani, H.R.; Borazjani, A.A.; Sinaei, M.; Hashemi, A. The Effect of Gas Injection on the Enhancement of Condensate Recovery in Gas Condensate Reservoirs: A Comparison between a Synthetic Model and PVT Cell Results. *Pet Sci Technol* **2014**, *32*, doi:10.1080/10916466.2011.596890.
40. Modebelu, E.C.; Nasriani, H.R.; Francis, J. Integrated Evaluation of the Clean-Up Performance of Unconventional Gas Plays; Investigating the Impact of Desiccation. In Proceedings of the 83rd EAGE Annual Conference & Exhibition; European Association of Geoscientists & Engineers, 2022; pp. 1–5.
41. Erimako, R.J.B.; Nasriani, H.R.; Asimakopoulou, E.; Graham, T.L.; Whitty, J. Numerical Investigation of Hydraulic Fractures in Multiple Horizontal Wells: Analysis of Zipper & Modified Zipper Fracking. In Proceedings of the 83rd EAGE Annual Conference & Exhibition; European Association of Geoscientists & Engineers, 2022; pp. 1–5.
42. Shi, Z.; Huang, Y.; Flottman, T.; Leonardi, C.; Lu, M.; Chen, Z. Characterization of Anisotropic Geomechanical Properties of Australian Bowen Basin Coals Through Nanoindentation and Upscaling Approaches. In Proceedings of the Day 2 Wed, November 15, 2023; SPE, November 12 2023.
43. Leonardi, C.R.; Di Vaira, N.J.; Laniewski-Wollk, L.; Ganpule, S.; Flottmann, T. Computational Analysis of Proppant Transport and Screen-Out in Natural and Induced Fractures. In Proceedings of the Day 2 Wed, November 15, 2023; SPE, November 12 2023.
44. Awan, F.U.R.; Keshavarz, A.; Akhondzadeh, H.; Al-Anssari, S.; Al-Yaseri, A.; Nosrati, A.; Ali, M.; Iglauer, S. Stable Dispersion of Coal Fines during Hydraulic Fracturing Flowback in Coal Seam Gas Reservoirs—An Experimental Study. *Energy & Fuels* **2020**, *34*, 5566–5577, doi:10.1021/acs.energyfuels.0c00045.
45. Leonardi, C.R.; Di Vaira, N.J.; Laniewski-Wollk, L.; Aminossadati, S.M.; Johnson, R.L. Probabilistic Quantification of Size Segregation and Screen-Out of Microparticles Subject to Electrostatic Forces. In Proceedings of the Day 1 Tue, January 31, 2023; SPE, January 24 2023.
46. Ramanandraibe, H.M.; Johnson, R.L.; Sedaghat, M.; Leonardi, C.R. Co-Application of Indirect Hydraulic Fracturing and Micro-Proppants with Existing Surface-to-Inseam Wells to Improve Pre-Drainage of Low Permeability Coals in Mining Areas. In Proceedings of the Day 3 Wed, October 04, 2023; SPE, October 2 2023.
47. Srinivasan, S.; O'Malley, D.; Mudunuru, M.K.; Sweeney, M.R.; Hyman, J.D.; Karra, S.; Frash, L.; Carey, J.W.; Gross, M.R.; Guthrie, G.D.; et al. A Machine Learning Framework for Rapid Forecasting and History Matching in Unconventional Reservoirs. *Sci Rep* **2021**, *11*, 21730, doi:10.1038/s41598-021-01023-w.
48. O'Meara Consulting Inc. Geo2Flow, Release 2014.5.4. *Geo2Flow* 2014.
49. Brooks, R.H.; Corey, A.T. Hydraulic Properties of Porous Media. **1964**.
50. Brooks, R.H.; Corey, A.T. Properties of Porous Media Affecting Fluid Flow. *Journal of the Irrigation and Drainage Division* **1966**, *92*, 61–90.
51. Bentsen, R.G.; Anli, J. Using Parameter Estimation Techniques To Convert Centrifuge Data Into a Capillary-Pressure Curve. **1977**, doi:10.2118/5026-PA.
52. Schlumberger Geoquest, ECLIPSE 100, Version 2015.1.0.0. *Simulation Launch Management Utility* 2015.

53. Thomas, L.K.; Katz, D.L.; Tek, M.R. Threshold Pressure Phenomena in Porous Media. *Society of Petroleum Engineers Journal* **1968**, *8*, 174–184.